


Confined Meson Excitations in Rydberg-Atom Arrays Coupled to a Cavity Field

Tharnier O. Puel^{1,2} and Tommaso Macrì^{3,2}

¹*Department of Physics and Astronomy, University of Iowa, Iowa City, Iowa 52242, USA*

²*Departamento de Física Teórica e Experimental, Universidade Federal do Rio Grande do Norte, Campus Universitário, Lagoa Nova, Natal-RN 59078-970, Brazil*

³*ITAMP, Harvard-Smithsonian Center for Astrophysics, Cambridge, Massachusetts 02138, USA*

 (Received 17 April 2024; revised 23 July 2024; accepted 30 July 2024; published 4 September 2024)

Confinement is a pivotal phenomenon in numerous models of high-energy and statistical physics. In this study, we investigate the emergence of confined meson excitations within a one-dimensional system, comprising Rydberg-dressed atoms trapped and coupled to a cavity field. This system can be effectively represented by an Ising-Dicke Hamiltonian model. The observed ground-state phase diagram reveals a first-order transition from a ferromagnetic-subradiant phase to a paramagnetic-superradiant phase. Notably, a quench near the transition point within the ferromagnetic-subradiant phase induces meson oscillations in the spins and leads to the creation of squeezed-vacuum light states. We suggest a method for the photonic characterization of these confined excitations, utilizing homodyne detection and single-site imaging techniques to observe the localized particles. The methodologies and results detailed in this Letter are feasible for implementation on existing cavity-QED platforms, employing Rydberg-atom arrays in deep optical lattices or optical tweezers.

DOI: [10.1103/PhysRevLett.133.106901](https://doi.org/10.1103/PhysRevLett.133.106901)

Introduction—The strong nuclear force bounds elementary particles with increasing strength with distance and appears between quarks to form, e.g., protons, neutrons, mesons, etc. Because of that, quarks are not found in isolation, a phenomenon called confinement. In condensed matter systems the confinement effect exists in low-dimensional-spin excitations [1–5], also referred to as meson excitations [2], and their presence are known to change qualitatively the spreading of correlations. Interestingly, such an effect was experimentally observed in the CaCu_2O_3 crystals probed by neutron scattering measurements and mathematically modeled by a weakly coupled spin ladder [6]. Neutron scattering was later used to observe confinement in the quasi-one-dimensional ferromagnet CoNb_2O_6 , and that could be well described by a transverse-field Ising model in the presence of a weak-longitudinal field [7]. More recently, advances in quantum technology allowed the creation and manipulation of confined spin excitations in a trapped-ion quantum simulator [8,9]. Recent studies have extended this understanding to include scattering events and dynamical formation of novel hadronic states in quantum spin chains with long-range interactions, opening new avenues in the simulation of quantum chromodynamics using trapped-ion or Rydberg-atom setups [10,11].

Our study introduces a novel approach to investigate confinement, employing a hybrid quantum device that utilizes a finite-range interacting spin chain coupled to a cavity field after a quantum quench. This method offers a fresh perspective on confinement dynamics, distinct from

previous studies. The experimental realization of the model involves neutral atoms, which are excited to Rydberg states via far-off-resonant processes [12–15]. This specific experimental setup has been proposed to explore and elucidate exotic many-body quantum phases [12,16–19]. Furthermore, this arrangement has shown promise for the generation of states with significant metrological applications [20–26]. The confinement of these Rydberg atoms is achieved through their localization in optical lattices [27] or within tweezer arrays with programmable geometries [28,29]. A pivotal aspect of this configuration is the interaction between the Rydberg atom arrays and a single mode of a cavity field which represents a significant advancement in understanding and controlling confined spin and photon excitations, a core novelty of our research.

Model and symmetries—The quantized transverse field Ising model (QTFIM) [30] combines two well-known models: the Ising and the Dicke model, $H_{\text{QTFIM}} = H_{\text{Ising}} + H_{\text{Dicke}}$. The one-dimensional (1D) Ising model describes the exchange interaction between spins positioned along a chain

$$H_{\text{Ising}} = -J_z \sum_n \sigma_n^z \sigma_{n+1}^z, \quad (1)$$

where $J_z > 0$ denotes the strength of the ferromagnetic interaction, and σ_n^z represents the z -spin projection of the n th spin. The Dicke model describes the light-matter interaction, specifically a single photon mode interacting uniformly with the spin chain as

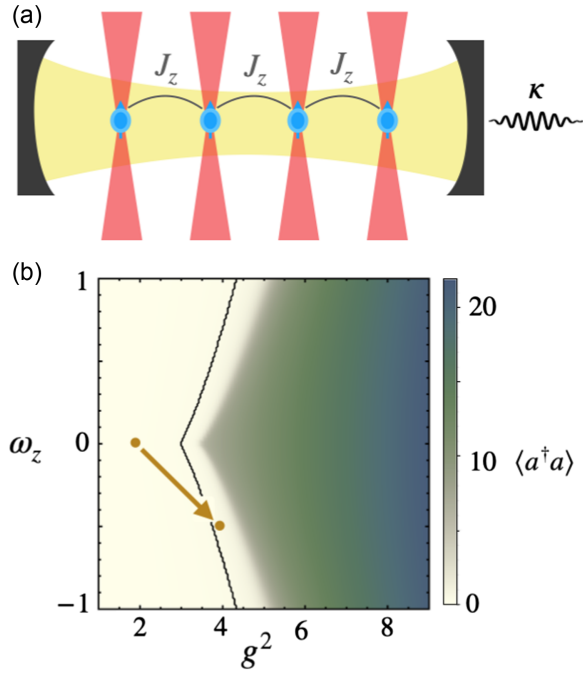


FIG. 1. (a) Illustration representing an array of atoms (blue) trapped by optical tweezers within an optical cavity with loss rate κ . (b) Phase diagram of the QTFIM for the spin-excitation frequency ω_z and spin-light interaction strength g . The colors represent the photon number $\langle a^\dagger a \rangle$, computed by exact diagonalization of H_{QTFIM} for $N_s = 10$ (truncating the photon basis to $N_p = 50$). The photon number is the order parameter for the transition between a ferromagnetic phase (with $\langle a^\dagger a \rangle = 0$ and $\langle \sigma_{z_0}^z \rangle = -1$) and a superradiant phase (with $\langle a^\dagger a \rangle \neq 0$ and $\langle \sigma_{z_0}^z \rangle \neq -1$). The black line indicates the phase transition obtained from the mean-field approach. The brown dots and arrow refer to the quench dynamics discussed in the main text.

$$H_{\text{Dicke}} = \omega_z S_z + \frac{g}{\sqrt{N_s}} (a^\dagger + a) S_x + \omega_a a^\dagger a, \quad (2)$$

where $S_\alpha \equiv \sum_i \sigma_i^\alpha / 2$ and N_s represents the total number of spins. The frequency splitting between atomic levels and the photon frequency are characterized by ω_z and ω_a , respectively. Note that, when combined, the $\omega_z S_z$ term acts as a longitudinal-magnetic field for the Ising model, whereas g represents the strength of a transverse-magnetic field for the spins. The cavity field is characterized by the quantized term $(a^\dagger + a)$, which distinctively differentiates this from the well-known transverse-field Ising model (TFIM). A similar model for light-matter interaction was studied in Ref. [31], where, instead, the coupling acts as an effective longitudinal-magnetic field for the spins.

The TFIM exhibits a Z_2 symmetry, $\sigma_n^z \rightarrow -\sigma_n^z$, leaving the Hamiltonian invariant. This symmetry is explicitly broken in the presence of the longitudinal field $\omega_z S_z$. The Dicke model is invariant under the simultaneous transformation $a \rightarrow -a$ and $S_x \rightarrow -S_x$. This symmetry results in vanishing magnetization along the x direction.

Phase diagram—The TFIM undergoes a second-order phase transition, induced by the transverse field, where the Z_2 symmetry is spontaneously broken leading to a ferromagnetic phase [32]. For vanishing ω_z , the QTFIM resembles the TFIM, with the transverse field being quantized via the operators $(a^\dagger + a)$. However, the QTFIM exhibits a first-order phase transition, whereby the increasing coupling strength g causes the system to transition from a ferromagnetic-subradiant phase (characterized by the absence of photon creation) to a paramagnetic-superradiant phase (where photons are collectively created by all spins) [30,33]. The complexity of the model increases substantially in the presence of an additional longitudinal field [34,35], with a well-defined phase diagram only known for a random distribution of the field [36–38]. Contrastingly, we show that the same does not apply to the QTFIM. Indeed, the first-order phase transition remains robust in the presence of $\omega_z (\neq 0)$.

From an exact diagonalization analysis of the H_{QTFIM} , we calculated the photon number $\langle a^\dagger a \rangle$ in the ground state for a range of values (ω_z, g^2) . The number of photons serves as the order parameter, being zero in the ferromagnetic phase and finite in the superradiant phase, see Fig. 1(b). See [39] for a detailed analysis of the phase transition point. Further insight into this transition is obtained from the mean-field treatment, as discussed in the following sections.

Mean field—The thermodynamic partition function can be approximated in the mean-field approach as

$$\begin{aligned} Z &= \lim_{N_s \rightarrow \infty} \text{Tr}[e^{-\beta H_{\text{QTFIM}}}], \\ &= \lim_{N_s \rightarrow \infty} \sqrt{\frac{N_s}{\beta\pi}} \int dx \exp[N_s f(x, m_z)], \end{aligned} \quad (3)$$

where

$$f(x, m_z) \equiv (-\beta\omega_a x^2 + \ln[2 \cosh(\beta\gamma/2)] - \beta J_z m_z^2), \quad (4)$$

and $x \equiv \text{Re}[\alpha]/\sqrt{N_s}$ with α denoting the photonic coherent state $a|\alpha\rangle = \alpha|\alpha\rangle$. We define $\gamma \equiv \sqrt{(2gx)^2 + (4J_z m_z - \omega_z)^2}$, representing the combined effects of interaction strengths and magnetization, with m_z being the magnetization along the z direction. See [39] for the complete derivation of Eq. (3). In the thermodynamic limit, Laplace's method [45,46] enables the determination of the optimal Gibbs-free energy by minimizing $f(x, m_z)$ with respect to x and m_z . The results are depicted in Fig. 2. A clear phase transition is evident, indicated by a discontinuity in x and m_z ; this discontinuity corresponds to the black line in Fig. 1(b).

Quench dynamics and confinement—Finite-system size effects tend to smooth the first-order mean-field transition curves into a continuous change of the order parameter and magnetization [39]. This phenomenon allows for a few spin

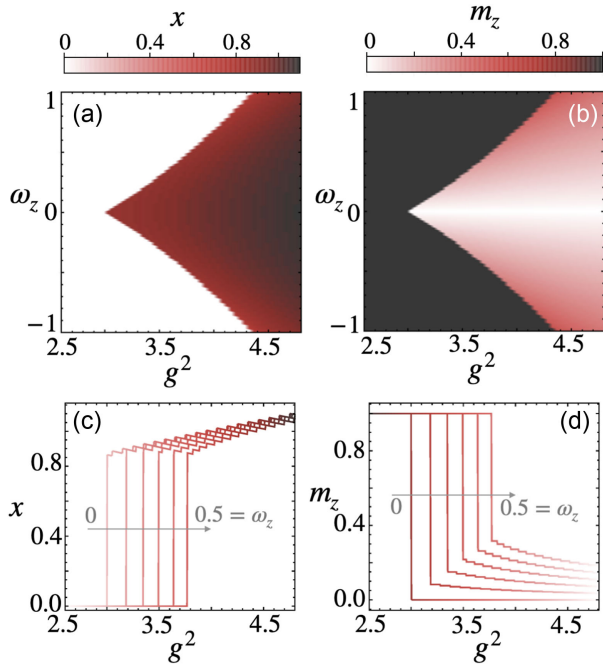


FIG. 2. The mean-field phase diagram for the (a) photon-coherent state x and (b) magnetization m_z as a function of the coupling strength g and the spin-excitation frequency ω_z . The transition is identified by the sudden change of colors, corresponding to the black line in Fig. 1(b). The lower plots show cuts (fixed values of ω_z) in the upper plots. Note that for $\omega_z = 0$, the magnetization m_z is zero on the right side of the transition. However, for $|\omega_z| > 0$, the m_z shifts from unity to a finite value; a similar, albeit slower, trend is observed for x .

flips and the emergence of a few photon modes near the transition line. In this study, we have examined the quench dynamics of spin excitations in the QTFIM near transition. Specifically, we start the system in the ferromagnetic phase and then abruptly shift it toward the transition line [this quench is represented in Fig. 1(b)] by increasing the spin-photon coupling g and introducing the frequency splitting ω_z . In a competing fashion, the parameter g facilitates spin flips in the z basis and photon creation, while ω_z promotes the alignment of all spins.

Similar to the TFIM, small clusters of spin excitations tend to remain confined within small regions, and the dynamics is characterized by oscillations in the size of these clusters. In the QTFIM, this dynamics can be tracked via the number of photons $\langle a^\dagger a \rangle(t)$ and the total magnetization $\langle \sigma_{r_0}^z \rangle(t)$ at time t , as shown in Fig. 3. We observe a decrease in the magnetization followed by an increase in the photon number. Also, the oscillations exhibit two characteristic frequencies, i.e., a fast oscillation modulated by a slower one. The fast oscillation is nearly insensitive to the system size, while the slower one is strongly dependent, as illustrated in Fig. 4. These frequencies can be determined by taking the Fourier transform

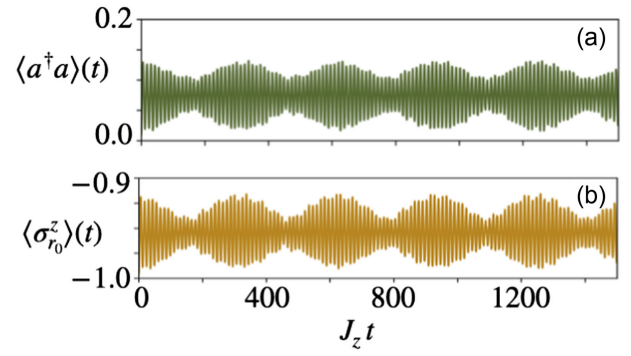


FIG. 3. Quench dynamics of the photon number and z magnetization, respectively, for $N_p = 30$ for the photon and $N_s = 14$ for the spin. We set $J_z = \omega_a$. The quench parameters are $(\omega_z, g^2) = (0, 2) \rightarrow (0.5, 4)$ and are signaled in Fig. 1. The dynamics are characterized by a rapid oscillation (with a period of $\Delta J_z t \approx 10$) modulated by a longer-period oscillation (with a period of $\Delta J_z t \approx 300$).

$$\langle a^\dagger a \rangle(\omega_n) = \frac{1}{\mathcal{N}} \sum_k e^{-i\omega_n t_k} \langle a^\dagger a \rangle(t_k), \quad (5)$$

where \mathcal{N} is the number of terms in the sum, $\omega_n/J_z = n$, and $J_z t_k = 2\pi k/\mathcal{N}$. The indexes run over $n, k = 1, 2, \dots, \mathcal{N}$. The fast oscillation frequency is discerned from the highest peak in the Fourier transformation, as depicted in Fig. 4(b). Confinement of spin excitations is evident by computing the connected correlation function (using periodic boundary conditions), $\langle \sigma_{r_0}^z \sigma_{r_0+r}^z \rangle_c \equiv \langle \sigma_{r_0}^z \sigma_{r_0+r}^z \rangle - \langle \sigma_{r_0}^z \rangle \langle \sigma_{r_0+r}^z \rangle$. Figure 4(c) shows a synchronized increase of the correlations with photon creation over time.

Characterization of the photonic field—We now turn our attention to analyzing the quench dynamics by examining the photonic properties. We compute the dynamics of the Wigner function of the photonic field, initially in a vacuum state, which is a Gaussian distribution centered at zero. We observe “breathing” oscillations of the Wigner function, which undergo oscillations and rotations in the phase space [47], as illustrated in Figs. 5(a) and 5(b).

We monitor the degree of squeezing, measurable by the function ζ_B [48]

$$\zeta_B^2 = 1 + 2(\langle a^\dagger a \rangle - |\langle a \rangle|^2) - 2|\langle a^2 \rangle - \langle a \rangle^2|. \quad (6)$$

The condition for squeezing is $\zeta_B^2 < 1$, as shown in Fig. 5(c). Additionally, we observe oscillations in the photon number distribution, attributed to interference in phase space between the ground and squeezed vacuum states [49,50], as shown in Fig. 5(f). The dynamics of the $g^{(2)}(\tau)$ correlation function [51]

$$g^{(2)}(\tau) = \frac{\langle a^\dagger(0) a^\dagger(\tau) a(\tau) a(0) \rangle}{\langle a^\dagger(0) a(0) \rangle^2}, \quad (7)$$

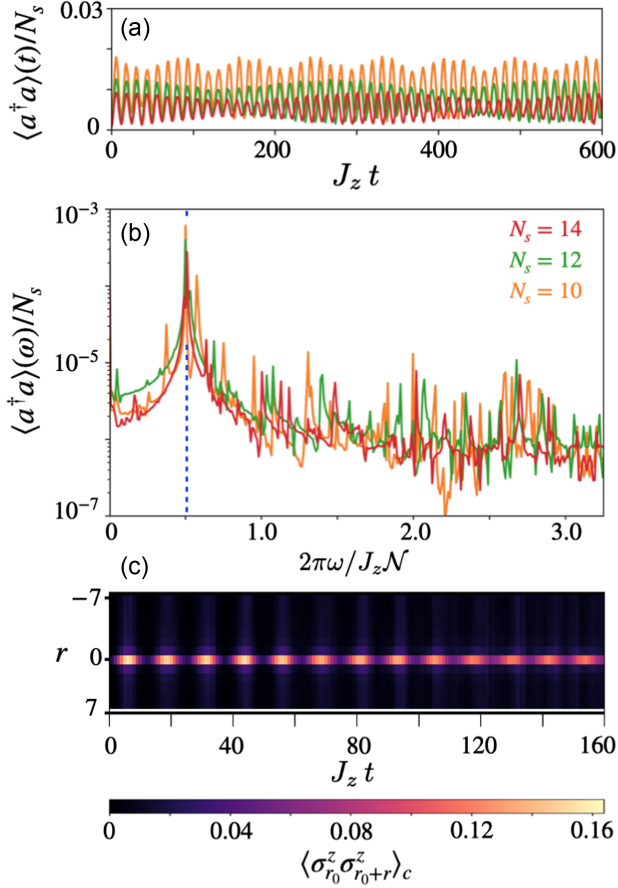


FIG. 4. (a) The same results as in Fig. 3(a) but for various system sizes. Note that the fast-oscillation period is nearly independent of the system size, while its modulation's period increases with the system size. The legends follow panel (b), which displays their respective Fourier transformation, with $\mathcal{N} = 3000$. The highest peak, indicated by the blue-vertical-dashed line, marks the frequency $\omega/J_z \approx 0.08N$ associated with the fast oscillation. (c) The connected spin-spin correlation function during the quench dynamics. Observe that the correlations remain short ranged in space (at a distance r between any two sites), indicating the confinement of the excitations, and that the correlation approaches zero every time the system nears the magnetic phase, with $\langle a^\dagger a \rangle = 0$. Periodic-boundary conditions were used for the exact diagonalization.

is depicted in Fig. 5(h). We note that $g^{(2)}(\tau) > g^{(2)}(0)$ for any time τ .

Open system dynamics—We express the master equation as $\partial_t \rho = -(i/\hbar)[H_{\text{QTFIM}}, \rho] + \mathcal{L}[\rho]$ [52,53], incorporating the Lindbladian

$$\mathcal{L}[\rho] = \gamma \sum_n \left(\sigma_n^- \rho \sigma_n^+ - \frac{1}{2} \{ \sigma_n^+ \sigma_n^-, \rho \} \right) + 2\kappa \left[a \rho a^\dagger - \frac{1}{2} \{ a^\dagger a, \rho \} \right], \quad (8)$$

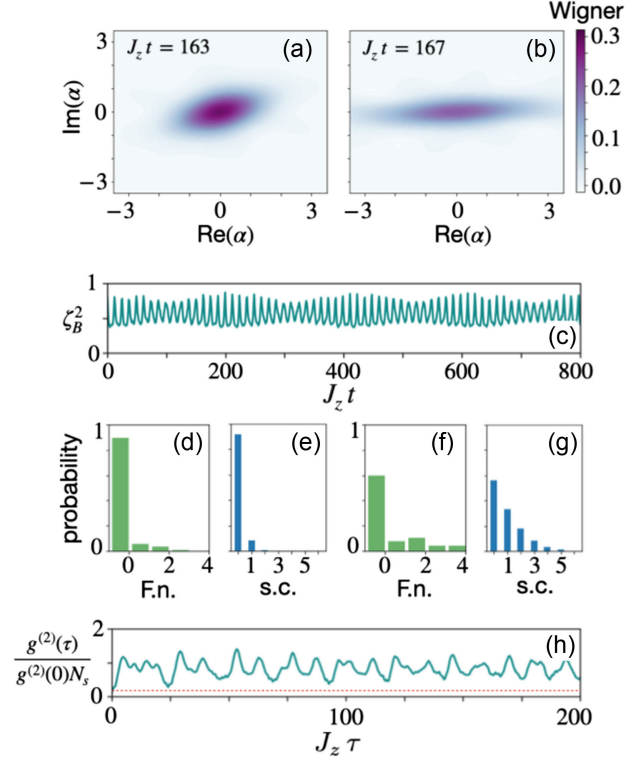


FIG. 5. Wigner function at $J_z t = 163$ (a) and $J_z t = 167$ (b) where the minimum and maximum photon excitation happen, respectively. The oscillation is accompanied by a squeezing in the photonic state. The squeezed vacuum state is characterized by the squeezing factor $\zeta_B^2 < 1$ shown in (c). For a better understanding of the photonic and magnetic states, we show the Fock number (F.n.) and the spin configuration (s.c.) in panels (d) and (e), respectively, for the same parameters as in (a). The (f) and (g) panels show analogous results but for the same parameters as in (b). Observe in panel (f) the pairwise creation of photons (0, 2, 4, ... photons), favoring over single photon creation. Finally, the quench is characterized by a correlation function $g^{(2)}(\tau) > g^{(2)}(0)$ at any instant τ , as seen in (h), where the red-dashed line is $1/N_s$ for $N_s = 6$.

with κ denoting the leakage rate and γ the atomic-decay rate. The first term accounts for independent atomic decay (σ_n^-), while the second term represents photon leakage from the cavity (a) due to imperfect mirrors, characterized by rate κ .

In Fig. 6, we examine these decay processes and compare the results with the dynamics of the closed system, using the same quench parameters as in Fig. 1(b). The closed system ($\gamma = \kappa = 0$) exhibits photon number and magnetization oscillations, consistent with the confinement effect described earlier. Including cavity leakage in the time evolution reveals that the confinement-induced oscillations are suppressed. Interestingly, the equilibrium state retains a finite photon number, indicating that the system remains in the superradiant phase. Conversely, atomic decay exerts a less dramatic effect on the dynamics, allowing the

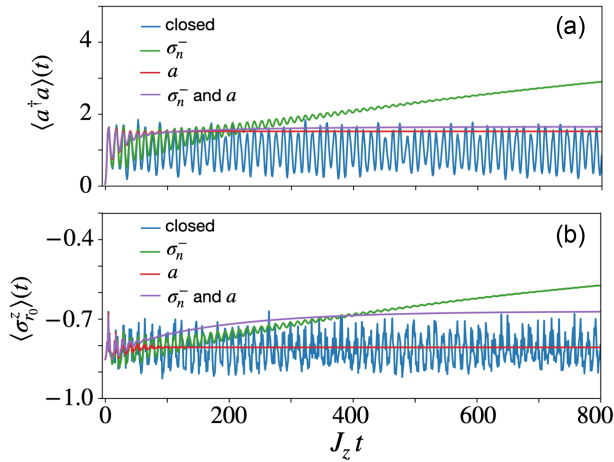


FIG. 6. (a) Photon number and (b) z magnetization of an open system for each one of the decay processes, described by the operators σ_n^- and a . The results are juxtaposed with the quench dynamics of the closed system (blue line), using the same parameters as in Fig. 1(b), with $N_s = 6$ and $N_p = 20$. The plots present four independent simulations: $\gamma = 0.01$, $\kappa = 0$ (green), $\gamma = 0$, $\kappa = 0.01$ (red), $\gamma = \kappa = 0.01$ (purple), and $\gamma = \kappa = 0$ (blue).

oscillations to persist and resulting in a longer equilibration time, and much higher photon number. When both effects are present, the cavity leakage dominates over the atomic decay, i.e., the oscillations are strongly suppressed and the system quickly converges to a steady state [39].

Conclusions—This study represents a significant advancement in the understanding of confinement dynamics in quantum spin systems, particularly in the context of their interaction with cavity fields. We have explored the equilibrium phase diagram and the dynamics of confinement in such systems. Our work integrates the effective spin-spin interactions among Rydberg atoms with the Dicke model in a cavity-assisted setting, paving the way for novel experimental investigations in quantum many-body physics.

The feasibility of this model is further underscored by its compatibility with existing experimental platforms, and the theoretical model is shown to be realizable with a Rydberg-dressed chain of atoms coupled to a cavity field. Finally, we highlight that the confinement effects unveiled in this research can be detected through optical readout, utilizing photon-cavity leakage, or via single-site imaging techniques. These methods are applicable to current experimental setups involving neutral-atom arrays, showcasing the broad applicability and potential impact of our findings in the field of quantum physics.

Acknowledgments—We acknowledge C. Dag, F. Liu, S. Ostermann, G. Pagano, and S. Yelin for useful discussions. This work was supported by the Serrapilheira Institute (Grant No. Serra-1812-27802). T. P. acknowledges

the hospitality of the Physics Department of UFRN and the Serrapilheira Institute for support. We thank the High-Performance Computing Center (NPAD) at UFRN for providing computational resources.

- [1] B. M. McCoy and T. T. Wu, *Phys. Rev. D* **18**, 1259 (1978).
- [2] P. Fonseca and A. Zamolodchikov, *J. Stat. Phys.* **110**, 527 (2003).
- [3] P. Fonseca and A. Zamolodchikov, [arXiv:hep-th/0612304](https://arxiv.org/abs/hep-th/0612304).
- [4] M. Kormos, M. Collura, G. Takács, and P. Calabrese, *Nat. Phys.* **13**, 246 (2017).
- [5] F. Liu, R. Lundgren, P. Titum, G. Pagano, J. Zhang, C. Monroe, and A. V. Gorshkov, *Phys. Rev. Lett.* **122**, 150601 (2019).
- [6] B. Lake, A. M. Tsvelik, S. Notbohm, D. Alan Tennant, T. G. Perring, M. Reehuis, C. Sekar, G. Krabbes, and B. Büchner, *Nat. Phys.* **6**, 50 (2010).
- [7] R. Coldea, D. A. Tennant, E. M. Wheeler, E. Wawrzynska, D. Prabhakaran, M. Telling, K. Habicht, P. Smeibidl, and K. Kiefer, *Science* **327**, 177 (2010).
- [8] W. L. Tan, P. Becker, F. Liu, G. Pagano, K. S. Collins, A. De, L. Feng, H. B. Kaplan, A. Kyprianidis, R. Lundgren, W. Morong, S. Whitsitt, A. V. Gorshkov, and C. Monroe, *Nat. Phys.* **17**, 742 (2021).
- [9] N. Defenu, T. Donner, T. Macri, G. Pagano, S. Ruffo, and A. Trombettoni, *Rev. Mod. Phys.* **95**, 035002 (2023).
- [10] J. Vovrosh, R. Mukherjee, A. Bastianello, and J. Knolle, *PRX Quantum* **3**, 040309 (2022).
- [11] Z. Wang, F. Wang, J. Vovrosh, J. Knolle, F. Mintert, and R. Mukherjee, [arXiv:2304.12623](https://arxiv.org/abs/2304.12623).
- [12] N. Henkel, R. Nath, and T. Pohl, *Phys. Rev. Lett.* **104**, 195302 (2010).
- [13] T. Macri and T. Pohl, *Phys. Rev. A* **89**, 011402(R) (2014).
- [14] A. Mitra, S. Omanakuttan, M. J. Martin, G. W. Biedermann, and I. H. Deutsch, *Phys. Rev. A* **107**, 062609 (2023).
- [15] Y. Y. Jau, A. M. Hankin, T. Keating, I. H. Deutsch, and G. W. Biedermann, *Nat. Phys.* **12**, 71 (2016).
- [16] T. Macri, F. Maucher, F. Cinti, and T. Pohl, *Phys. Rev. A* **87**, 061602(R) (2013).
- [17] S. Hollerith, K. Srakaew, D. Wei, A. Rubio-Abadal, D. Adler, P. Weckesser, A. Kruckenhauser, V. Walther, R. van Bijnen, J. Rui, C. Gross, I. Bloch, and J. Zeiher, *Phys. Rev. Lett.* **128**, 113602 (2022).
- [18] T. Macri, S. Saccani, and F. Cinti, *J. Low Temp. Phys.* **177**, 59 (2014).
- [19] F. Cinti, T. Macri, W. Lechner, G. Pupillo, and T. Pohl, *Nat. Commun.* **5**, 3235 (2014).
- [20] E. Davis, G. Bentsen, and M. Schleier-Smith, *Phys. Rev. Lett.* **116**, 053601 (2016).
- [21] T. Macri, A. Smerzi, and L. Pezzè, *Phys. Rev. A* **94**, 010102 (R) (2016).
- [22] R. Kaubruegger, P. Silvi, C. Kokail, R. van Bijnen, A. M. Rey, J. Ye, A. M. Kaufman, and P. Zoller, *Phys. Rev. Lett.* **123**, 260505 (2019).
- [23] V. Borish, O. Marković, J. A. Hines, S. V. Rajagopal, and M. Schleier-Smith, *Phys. Rev. Lett.* **124**, 063601 (2020).
- [24] J. A. Hines, S. V. Rajagopal, G. L. Moreau, M. D. Wahrman, N. A. Lewis, O. Marković, and M. Schleier-Smith, *Phys. Rev. Lett.* **131**, 063401 (2023).

- [25] J. T. Young, S. R. Muleady, M. A. Perlin, A. M. Kaufman, and A. M. Rey, *Phys. Rev. Res.* **5**, L012033 (2023).
- [26] W. J. Eckner, N. Darkwah Oppong, A. Cao, A. W. Young, W. R. Milner, J. M. Robinson, J. Ye, and A. M. Kaufman, *Nature (London)* **621**, 734 (2023).
- [27] J. Gelhausen, M. Buchhold, A. Rosch, and P. Strack, *SciPost Phys.* **1**, 004 (2016).
- [28] H. Bernien, S. Schwartz, A. Keesling, H. Levine, A. Omran, H. Pichler, S. Choi, A. S. Zibrov, M. Endres, M. Greiner, V. Vuletić, and M. D. Lukin, *Nature (London)* **551**, 579 (2017).
- [29] H. Labuhn, D. Barredo, S. Ravets, S. de Léséleuc, T. Macrì, T. Lahaye, and A. Browaeys, *Nature (London)* **534**, 667 (2016).
- [30] J. Rohn, M. Hörmann, C. Genes, and K. P. Schmidt, *Phys. Rev. Res.* **2**, 023131 (2020).
- [31] B. Zhu, J. Marino, N. Y. Yao, M. D. Lukin, and E. A. Demler, *New J. Phys.* **21**, 073028 (2019).
- [32] E. Barouch and B. M. McCoy, *Phys. Rev. A* **3**, 786 (1971).
- [33] P. Nevado and D. Porras, *Phys. Rev. A* **92**, 013624 (2015).
- [34] Y. Y. Atas and E. Bogomolny, *J. Phys. A* **47**, 335201 (2014).
- [35] Y. Y. Atas and E. Bogomolny, *J. Phys. A* **50**, 385102 (2017).
- [36] Y.-Q. Wang and Z.-Y. Li, *J. Phys. Condens. Matter* **6**, 10067 (1994).
- [37] O. Canko and E. Albayrak, *Phys. Lett. A* **340**, 18 (2005).
- [38] B. K. C. Sei Suzuki and Jun-ichi Inoue, *Quantum Ising Phases and Transitions in Transverse Ising Models*, Lecture Notes in Physics Vol. 862 (Springer, New York, 2012).
- [39] See Supplemental Material at <http://link.aps.org/supplemental/10.1103/PhysRevLett.133.106901>, which includes Refs. [40–44], for additional information about the derivation of the expressions, additional numerical simulations, and detailed discussion of the experimental realization of the model.
- [40] D. A. Steck, Rubidium 87D Line Data, Available online at <http://steck.us/alkalidata> (2023).
- [41] Z. Zhiqiang, C. H. Lee, R. Kumar, K. J. Arnold, S. J. Masson, A. S. Parkins, and M. D. Barrett, *Optica* **4**, 424 (2017).
- [42] L. Béguin, A. Vernier, R. Chicireanu, T. Lahaye, and A. Browaeys, *Phys. Rev. Lett.* **110**, 263201 (2013).
- [43] D. Barredo, S. Ravets, H. Labuhn, L. Béguin, A. Vernier, F. Nogrette, T. Lahaye, and A. Browaeys, *Phys. Rev. Lett.* **112**, 183002 (2014).
- [44] N. Šibalić, J. Pritchard, C. Adams, and K. Weatherill, *Comput. Phys. Commun.* **220**, 319 (2017).
- [45] C. F. Lee and N. F. Johnson, *Phys. Rev. Lett.* **93**, 083001 (2004).
- [46] S. Gammelmark and K. Mølmer, *New J. Phys.* **13**, 053035 (2011).
- [47] W. P. Schleich, *Quantum Optics in Phase Space* (John Wiley and Sons, New York, 2011).
- [48] J. Ma, X. Wang, C. Sun, and F. Nori, *Phys. Rep.* **509**, 89 (2011).
- [49] W. Schleich and J. A. Wheeler, *Nature (London)* **326**, 574 (1987).
- [50] G. Breitenbach, S. Schiller, and J. Mlynek, *Nature (London)* **387**, 471 (1997).
- [51] M. O. Scully and M. S. Zubairy, *Quantum Optics* (Cambridge University Press, Cambridge, England, 1997).
- [52] J. Johansson, P. Nation, and F. Nori, *Comput. Phys. Commun.* **183**, 1760 (2012).
- [53] J. Johansson, P. Nation, and F. Nori, *Comput. Phys. Commun.* **184**, 1234 (2013).